FUDMA Journal of Sciences (FJS)
ISSN online: 2616-1370
ISSN print: 2645 - 2944
Vol. 10 No. 14, July, 2026, pp 132 – 138
DOI: https://doi.org/10.33003/fjs-2026-1014-5722

Effect of Calcination Temperature on the Structural, Optical, and Photocatalytic Properties of Urea-Derived g-C_3N_4 for Methylene Blue Degradation

Usman Adamu, *Saidu Usman, Ibrahim Yusuf and Aisha Musa Aminu

Department of Chemistry, Sule Lamido University, Kafin Hausa, Jigawa State, Nigeria.

*Corresponding authors' email: usman.said@slu.edu.ng

Received: 27 Jul. 2026
Accepted: 09 Aug. 2026
Published: 17 Aug. 2026

ABSTRACT
Graphitic carbon nitride (g-C_3N_4) stands out as an eco-friendly, metal-free photocatalyst for the remediation of dye-contaminated wastewater. Though its efficiency relies heavily on its synthesis conditions. Pristine g-C_3N_4 was synthesized by thermally polymerizing urea at 500, 550, and 600℃, producing samples designated as GCN-500, GCN-550, and GCN-600, respectively. The effect of calcination temperature on the structural, morphological, optical, and photocatalytic properties of the synthesized materials was systematically investigated. FTIR and XRD analyses confirmed the formation of the characteristic g-C_3N_4 framework, while SEM revealed temperature-dependent morphological changes. The optical band gap energies of GCN-500, GCN-550, and GCN-600 were estimated as 2.89, 2.71, and 2.82 eV, respectively. The photocatalytic activity was evaluated through the visible-light degradation of methylene blue (MB). GCN-550 exhibited the highest photocatalytic performance, achieving approximately 90% MB degradation within 60 mins, compared with 58% and 68% for GCN-500 and GCN-600, respectively. The corresponding apparent rate constant of GCN-550 ($0.0352 min^{-1}$) was substantially higher than those of GCN-500 ($0.0142 min^{-1}$) and GCN-600 ($0.0194 min^{-1}$). Scavenging experiments indicated that superoxide radicals were the dominant reactive species, while hydroxyl radicals and photogenerated holes also contributed to MB degradation. Furthermore, GCN-550 retained approximately 78% degradation efficiency after four consecutive cycles. Generally, calcination at 550 ℃ produced g-C_3N_4 with optimized structural and optical properties, resulting in enhanced photocatalytic performance and promising reusability for dye-contaminated wastewater treatment.

Keywords: Graphitic carbon nitride, methylene blue, dye degradation, photocatalysis, wastewater treatment

INTRODUCTION

Wastewater from textile, paper, and garment factories often contains organic dyes that pose a serious environmental threat. These dye-laden effluents are not only hazardous and non-biodegradable but also contain carcinogenic pigments that can harm both ecosystems and human health (Donolikar *et al*., 2025). Methylene blue (MB) and other cationic dyes are commonly used as colorants in many industries, especially in textile dyeing and printing. Because of their widespread application, these dyes frequently end up contaminating water bodies (Rasheed *et al*., 2024; Tibebu *et al*., 2025). What makes MB particularly concerning is its chemical structure, which contains an azo linkage (–N=N–) known to be linked to carcinogenic effects (Eswaran *et al*., 2025). When ingested or exposed to in high amounts, MB can cause a range of health problems in humans, including respiratory difficulties, neurological issues, gastrointestinal distress, headaches, nausea, abdominal pain, blurred vision, dizziness, and even anemia (Nabeel *et al*., 2025). It is also highly toxic to aquatic life, disrupting ecosystems and harming fish and other organisms (Islam *et al*., 2026). Due to these serious environmental and health risks, various treatment methods have been developed and applied to remove methylene blue from wastewater. These include bio-adsorption, aerobic treatment, ion exchange, coagulation, membrane filtration, and photocatalytic degradation (Donolikar *et al*., 2025).

Over the past few decades, photocatalysis has become a well-established and widely used technique for the degradation of environmental pollutants (Anwer *et al*., 2019). This effectiveness is largely attributed to the generation of highly reactive oxidizing species, which can attack and mineralize a broad spectrum of organic contaminants (Rafiq *et al*., 2021). Recently, Graphitic carbon nitride (g-C_3N_4) has gained significant attention as a promising photocatalyst due to its unique combined advantages, such as natural abundance, metal-free composition, low toxicity, cost-effectiveness, and strong stability under ambient conditions (Sewnet *et al*., 2023). Additionally, it possesses a relatively narrow bandgap of approximately 2.7 eV, which enables it to efficiently absorb visible light and deliver strong photocatalytic performance (Wudil *et al*., 2023). One of the most crucial reaction factors that affects the effectiveness of graphitic carbon nitride (g-C_3N_4) is regulating the calcination temperature. As a result, altering the calcination temperature during synthesis can expand visible-light absorption, increase surface area, improve crystallinity, and eventually increase overall photocatalytic performance (Sewnet *et al.*, 2023).

Although g-C_3N_4 has been extensively investigated, a large proportion of reported studies have focused on enhancing its performance through doping, surface modification, or composite formation, while pristine g-C_3N_4 is often employed primarily as a reference material (Ke *et al*., 2022). Calcination temperature is a critical parameter that governs the degree of polymerization, crystallinity, surface area, and electronic structure of g-C_3N_4, all of which directly influence its photocatalytic efficiency (Donolikar *et al*., 2025; Michalska *et al*., 2024). In this study, g-C_3N_4 was synthesized via the

thermal polymerization of urea at three different calcination temperatures (500℃, 550℃, and 600℃) to systematically investigate the effect of thermal treatment on its physicochemical properties and photocatalytic performance. The photocatalytic activity of the as-prepared materials was evaluated through the degradation of methylene blue (MB) under visible light irradiation. By correlating structural and optical characteristics with photocatalytic behaviour, this work seeks to elucidate how subtle variations in calcination temperature can be used to tune the performance of g-C_3N_4. The findings are expected to contribute to the rational design of efficient, metal-free photocatalysts for dye-contaminated wastewater treatment.

MATERIALS AND METHODS

Materials:

Urea (CH_4N_2O), methylene blue (MB), isopropanol (IPA), ascorbic acid (AA), ethylene diamine tetraacetic (EDTA), and ethanol, were of analytical grade. All reagents were used as received without further purification.

Synthesis of g-C_3N_4

Pristine graphite carbon nitride (g-C_3N_4) was synthesized according to the procedure reported by Zheng *et al.* (2025), with some modifications. In a typical synthesis, 15g of urea was placed into a semi-closed alumina crucible, which was then placed into a muffle furnace and subjected to calcination at 500℃ for 120 min (5℃/min heating rate). After the crucible had cooled to ambient temperature, the resulting samples were collected and crushed into a fine powder using a mortar and pestle. The as-synthesized pristine g-C_3N_4 was labelled as GCN-500, corresponding to the calcination temperature used. Similarly, GCN-550, and GCN-600 were produced in the same manner at 550℃ and 600℃, respectively.

Characterizations

The FTIR analysis of the synthesized g-C_3N_4 was conducted using an Agilent Cary 630 FTIR spectrophotometer (Agilent Technologies, Malaysia) in the wavenumber range of 4000-400 cm^{-1} at a resolution of 16 cm^{-1} and 64 scans. The crystalline structure was examined using a Philips X'Pert diffractometer (Model: PW3040/60 X'Pert PRO MPD, Netherlands), with Cu–Kα radiation (λ = 0.15478 nm), over a 2θ range of 10-70°. The surface morphology was studies using scanning electron microscopy (SEM,) with a Phenom ProX Scanning Electron Microscope (Model: 800–07334, Phenom World, Netherlands). The UV-Vis absorption spectra of the synthesized materials were recorded using a Cary 60 UV-Vis spectrophotometer (Agilent Technologies, USA) over the wavelength range of 200–800 nm. The combined use of FTIR, XRD, and UV-Vis spectroscopy is well established for characterizing the structural and optical properties of synthesized nanomaterials for catalytic applications (Danbature *et al*., 2024).

Photocatalytic Experiment

The photocatalytic activity of the synthesized photocatalysts was evaluated in a photodegradation experiment comprising 100 mL of 10 mg/L MB solution as a target pollutant using homemade reactor fitted with two fluorescent bulbs (10 W). Initially, 0.03 g of the photocatalyst was dispersed into the MB solution and stirred in the dark for 30 min to achieve adsorption–desorption equilibrium, before irradiation. At predetermined time intervals, 2 mL of the solution was taken and centrifuge for 10min and the degradation was observed by measuring the absorbance at lambda max of 664 nm using a UV-Vis spectrophotometer (Biobase LLC, 3231 Osgood common Fremont, CA94539, and USA). The MB degradation percentage, R (%), was calculated using Equation (1), while, the reaction kinetics were analyzed using the modified Langmuir–Hinshelwood model (Equation (2)) (Roškaric *et al*., 2022)

$$R\ (\%) = \frac{C_0 - C_t}{C_0} \quad (1)$$

$$-\ln\left(\frac{C_t}{C_0}\right) = \text{kt} \quad (2)$$

Where, C_0 represents the concentration before light irradiation, C_t is the concentration at a determined reaction time, k is the degradation rate constant, and t is the reaction time (min).

RESULTS AND DISCUSSION

Characterizations

FTIR study

FTIR spectroscopy was used to identify the functional group of prepared g-C_3N_4 samples. As presented in Fig 1(a – c), all samples exhibit the characteristic absorption bands of graphitic carbon nitride, confirming the successful polymerization of urea into the g-C_3N_4 framework. The broad absorption band between $3357\ cm^{-1}$ and $3025\ cm^{-1}$ is associated to the stretching vibrations of terminal N–H groups (Wang *et al*., 2019). The bands observed at 1629 cm^{-1} and 1554 cm^{-1} can be assigned to the stretching vibrations of C=N bonds within the conjugated aromatic heterocyclic units. The series of bands appearing in the 1454 – 1235 cm^{-1} region are characteristic stretching vibrations of C–N bonds in the bridging nitrogen-containing units, including C–N(–C)–C and C–NH–C linkages. At lower wavenumbers, the absorptions around 884 and 809 cm^{-1} are related to the characteristic bending modes of the tri-s-triazine and s-triazine structural units, respectively, which are the characteristic fingerprints of g-C_3N_4 (Nabeel *et al.*, 2026; Pourali *et al*., 2025). The progressive enhancement of the characteristic C–N and C=N vibrational bands with increasing synthesis temperature suggests a greater degree of condensation and development of the g-C_3N_4 framework.

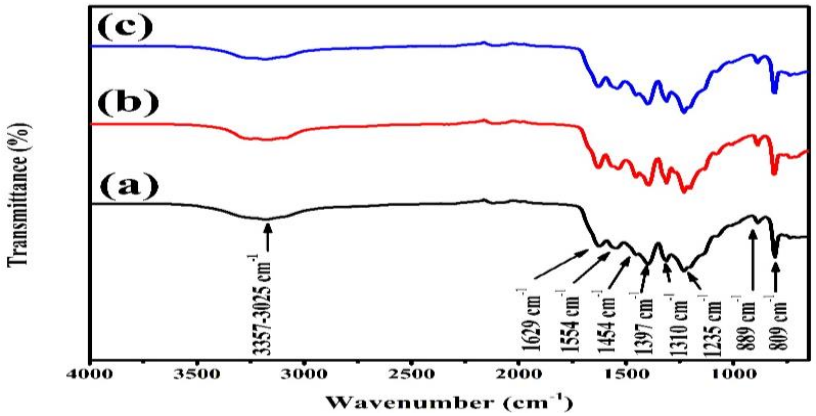

Figure 1: The FTIR spectra of (a) GCN-500 (b) GCN-550 and (c) GCN-600

XRD Study

X-ray diffraction method was employed for the evaluation of phase and crystallinity of the synthesized g-C_3N_4 samples. The XRD patterns (Fig. 2) displayed two characteristic reflections at around 2θ values, $13.1°$ and$27.2 - 27.7°$, assigned to the (100) and (002) planes of g-C_3N_4, respectively. The former is associated with the in-plane structural packing of the tri-s-triazine units, while the latter corresponds to the interlayer stacking of the conjugated g-C_3N_4 layers (Gu *et al*., 2015). The absence of additional prominent diffraction peaks suggests the formation of predominantly g-C_3N_4 without detectable crystalline secondary phases. The (002) peak shifted slightly from 27.2° for GCN-500 (Fig. 2a) to 27.7° for GCN-550 and GCN-600 (Figs. 2b and c), indicating a slight decrease in interlayer spacing of the g-C_3N_4 layers at higher synthesis temperatures (Parmar *et al*., 2026). In addition, the intensities of the characteristic diffraction peaks increased progressively from GCN-500 to GCN-600, with a more pronounced increase between GCN-500 and GCN-550. This suggests enhanced structural ordering and progressive polycondensation of the g-C_3N_4 framework with increasing synthesis temperature (Speltini *et al*., 2018; Parmar *et al*., 2026). The trend is consistent with the FTIR results, which also showed increasing intensities of the characteristic C–N/C=N vibrations, further indicating the development of the condensed g-C_3N_4 network at higher temperatures.

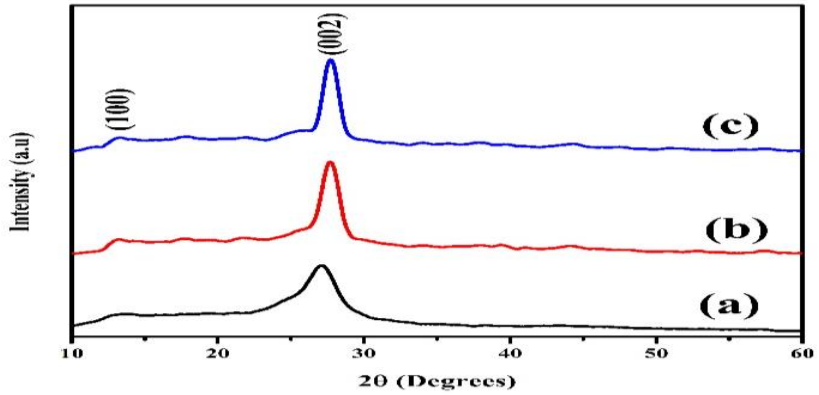

Figure 2: The XRD spectra of (a) GCN-500 (b) GCN-550 and (c) GCN-600

Morphology study

The surface morphology of the samples was examined by scanning electron microscopy (SEM), and the image are shown in Fig. 3(a – c). All samples showed irregular, agglomerated particles with rough surfaces, which are characteristic of g-C_3N_4 prepared by the thermal polymerization of urea (Alwin *et al*., 2020). Significant morphological differences were found with increasing calcination temperature. GCN-500 (Fig. 3a) exhibit densely packed and irregular aggregates, showing incomplete thermal condensation and low exposure of active sites. In contrast, GCN-550 (Fig. 3b) showed a more homogeneous particle distribution with relatively loose agglomeration and increased interparticle pores, offering a more favourable morphology for light absorption and the diffusion of reactant molecules. However, GCN-600 (Fig. 3c) exhibit larger and more compact agglomerates, which results from excess thermal treatment, resulted to particle growth and decrease in the accessible surface area (Donolikar *et al*., 2025). These structural changes indicate that GCN-550 possesses a more favourable textural profile among the synthesized photocatalysts, combining moderate particle size with increased porosity and surface exposure, features generally associated with improved light harvesting and charge carrier separation in g-C_3N_4-based materials (Michalska *et al*., 2024).

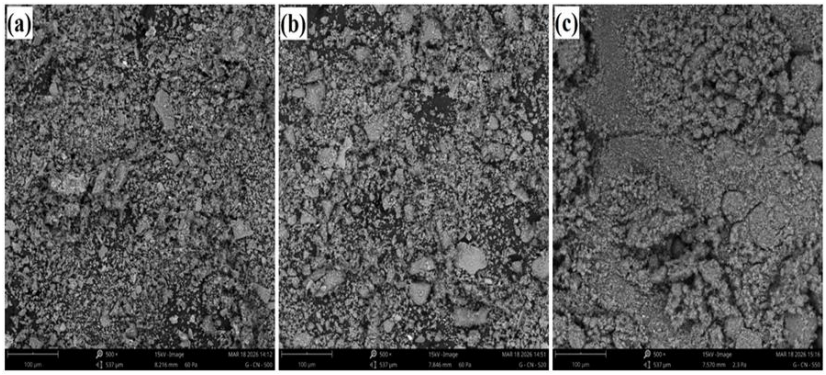

Figure 3: The SEM images of (a) GCN-500 (b) GCN-550 and (c) GCN-600

Band Gap Analysis

The optical properties of the synthesized g-C_3N_4 photocatalysts were examined using UV–Vis absorption spectroscopy, and the corresponding spectra are presented in Fig. 4(a). The absorption edges of the samples exhibited a temperature-dependent shift, initially red-shifting toward longer wavelengths as the calcination temperature increased from 500 to 550 ℃, followed by a blue-shift toward shorter wavelengths at 600 ℃, indicating that thermal treatment significantly affects the electronic structure and light-harvesting ability of g-C_3N_4 (Donolikar *et al*., 2025). The optical band gap energies were assessed from the Tauc's plot (Fig. 4(b)) using equation (3) (Mallik & Rath, 2022).

$$(\propto h\nu)^n = A(h\nu - E_g) \qquad (3)$$

Where: α = absorption coefficient, h = Planck's constant, v = frequency, n = 1/2 or 2 for direct or indirect transitions, respectively, A = constant, and Eg = band gap energy. The computed band gap energies for GCN-500, GCN-550, and GCN-600 were 2.89, 2.71, and 2.82 eV, respectively. As the calcination temperature increased from 500 ℃ to 550 ℃, the band gap decreased from 2.89 to 2.71 eV, indicating an improved degree of thermal condensation and enhanced π-electron delocalization within the heptazine framework (Donolikar *et al*., 2025). This structural evolution facilitates visible-light absorption by reducing the energy required to excite electrons from the valence band to the conduction band. Further increasing the calcination temperature to 600 ℃ resulted in a slight broadening of the band gap to 2.82 eV. This behavior is likely associated with excessive thermal treatment which may induce structural defects, partial disruption of the conjugated network, or a reduction in the effective conjugation length of the g-C_3N_4 framework (Paul *et al.*, 2019). The enhanced optical response of GCN-550 is expected to promote the generation, separation, and migration of photogenerated charge carriers, thus improving photocatalytic efficiency.

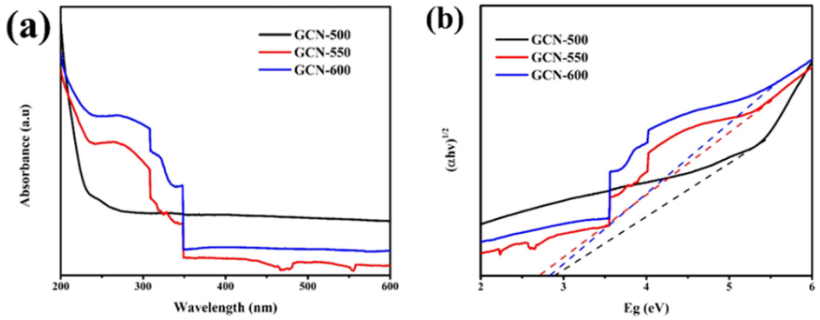

Figure 4: (a) UV-Vis Absorption spectra, and (b) the estimated band gap energies of the synthesized GCN photocatalysts

Photocatalytic Activity

The photocatalytic activity of the synthesized samples was evaluated on the degradation of methylene blue (MB) dye under visible-light irradiation, and results are shown in Fig 5(a). Control experiments performed in the absence of photocatalyst (photolysis) and under dark conditions (adsorption) showed an insignificant MB removal of about 5% and 17%, respectively, showing that neither direct photolysis nor adsorption alone helped significantly to dye removal. These observations confirm that the degradation of MB generally occurred over photocatalytic reactions under visible-light irradiation. As presented in Fig 5(a), the photocatalytic activity of prepared samples strongly depended on the calcination temperature. Among the three photocatalysts, GCN-550 shown the best photocatalytic activity, obtaining approximately 90% degradation of MB within 60 mins. In comparison, GCN-600 and GCN-500 removed approximately 68% and 58% of the dye, respectively. The superior performance of GCN-550 can be attributed to its optimized structural and electronic properties, such as improved crystallinity, enhanced visible-light absorption, efficient separation of photo generated electron-hole pairs, and a larger number of accessible active sites. Whereas, relatively lower activity of GCN-500 may be due to the incomplete condensation during synthesis, while the decreased performance of GCN-600 is due to excessive thermal treatment, which can decrease the surface area and introduce structural defects that promote charge recombination. Similar findings were reported by Parmar *et al*. (2026).

The photocatalytic degradation kinetics was examined using the modified Langmuir-Hinshelwood model, and the plots are presented in Fig 5(b). All samples showed excellent linear relationships with correlation coefficients (R^2) greater than 0.99, indicating that the degradation process follows pseudo-first-order kinetics. The calculated apparent rate constants (k)

followed the order: GCN-550 (0.0352 min^{-1}) > GCN-600 (0.0194 min^{-1}) > GCN-500 (0.0142 min^{-1}) > adsorption (0.0034 min^{-1}) > photolysis (0.0009 min^{-1}). Notably, the apparent rate constant of GCN-550 is approximately 39-folds greater than that of photolysis alone, showing its outstanding photocatalytic efficiency under visible-light irradiation. The kinetic results agree well with the degradation efficiencies observed in Fig. 5(a), confirming calcination at 550 ℃ gives the optimum conditions for producing g-C_3N_4 with better photocatalytic performance.

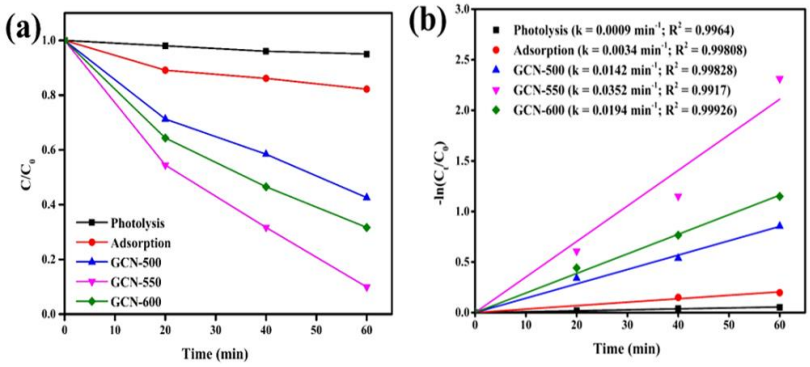

Figure 5: (a) Photocatalytic degradation of MB using the synthesized GCN photocatalysts (b) kinetic curve evaluating the rate constants

Scavenging Test

To identify the reactive species responsible for the photocatalytic degradation of MB, scavenging tests were conducted using isopropanol (IPA), ethylenediaminetetraacetic acid (EDTA), and ascorbic acid (AA) as scavengers for hydroxyl radicals (•OH), photogenerated holes (h^+), and superoxide radicals ($O_2^{\bullet-}$), respectively. As shown in Fig. 6(a), in the absence of any scavenger, the GCN-550 photocatalyst achieved almost 90% degradation of MB solution after 60 mins of visible-light irradiation, which served as the reference for comparison. The addition of IPA and EDTA noticeably reduced the degradation efficiency to almost 44% and 48%, respectively, showing both hydroxyl radicals and photogenerated holes participate in the photocatalytic degradation process. However, the most significant suppression was observed by addition of AA, at which the degradation efficiency reduced to almost 28%. This pronounced inhibition show superoxide radical ($O_2^{\bullet-}$) is the major reactive species responsible for MB degradation, while hydroxyl radicals (•OH) and holes (h^+) play important roles in the photocatalytic reaction.

Reusability Study

The reusability of the optimized GCN-550 photocatalyst were further observed through four continuous photocatalytic degradation cycles, as presented in Fig. 6(b). The degradation efficiency reduced from 90% in first cycle to 78% in the fourth cycle. Though a marginally reduction in photocatalytic activity was revealed after repeated use, the catalyst maintained a high level of degradation efficiency during the recycling tests. The observed decrease in the efficiency may be associated with the partial loss of catalyst during the retrieval process and the aggregation of degradation intermediates on the catalyst surface, which may block active sites and decrease photocatalytic performance. The GCN-550 photocatalyst show good structural stability and satisfactory reusability, highlighting its suitability for practical wastewater treatment applications.

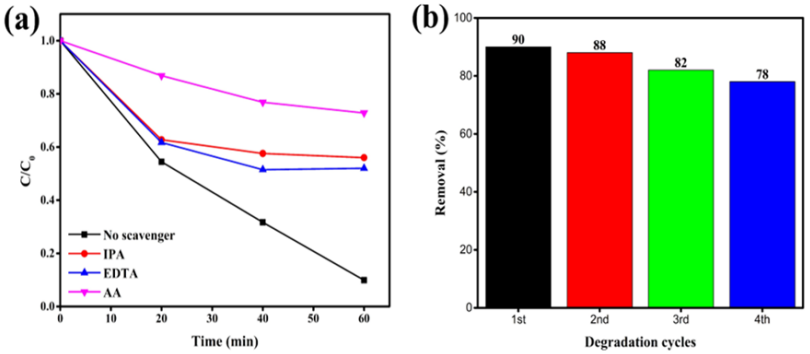

Figure 6: (a) Scavenging experiment (b) reusability study

Proposed Degradation Mechanism

Based on the results of the radical scavenging test a plausible mechanism for the visible-light-driven degradation of MB dye over GCN-550 photocatalyst was proposed. Upon light irradiation, g-C_3N_4 photocatalyst absorbs light greater than or equal to its band gap energy. Leading to production of photogenerated electrons (e^-) in the conduction band (CB) as well as holes (h^+) in the valence band (VB) (Eq. 4). While the electrons in the CB reacts with the dissolved oxygen to form superoxide radicals ($O_2^{\bullet-}$) (Eq. 5), the photogenerated holes in the VB either directly oxidize MB or react with water and surface hydroxyl ions to produce hydroxyl radicals (•OH) (Eq. 6). These reactive species thereafter strike the dye molecules, resulting in the split of the chromophoric structure, creation of the intermediate products, and their eventual mineralization into CO_2, H_2O, and other harmless inorganic products (Eq. 7). The overall process is schematically presented in Fig. (7)

$$g\text{-}C_3N_4 + hv \rightarrow e^-_{CB} + h^+_{VB} \quad (4)$$

$$e^-_{CB} + O_2 \rightarrow {}^{\bullet}O_2^- \quad (5)$$

$$h^+_{VB} + H_2O/OH^- \rightarrow {}^{\bullet}OH \quad (6)$$

$${}^{\bullet}O_2^- + {}^{\bullet}OH + MB \rightarrow CO_2 + H_2O + \text{inorganic ions} \quad (7)$$

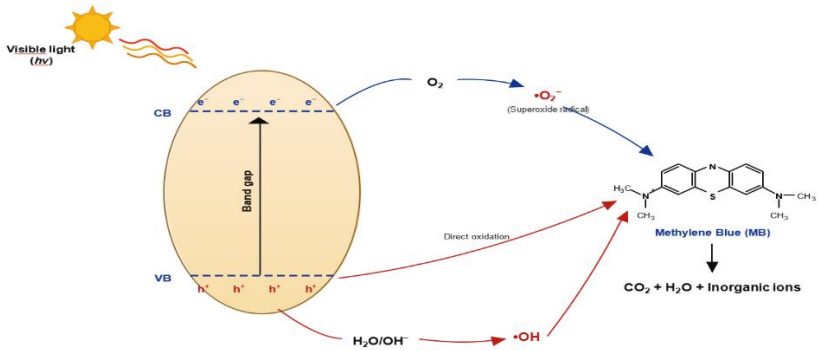

Figure 7: Schematic representation of the photocatalytic degradation of the MB dye, using GCN-550 photocatalyst under visible light irradiation

CONCLUSION

In this study, pristine g-C_3N_4 photocatalysts were successfully synthesized from urea at different calcination temperatures, and the influence of thermal treatment on their physicochemical and photocatalytic properties was investigated. The results demonstrated that calcination temperature significantly affected the structural, morphological, and optical characteristics of g-C_3N_4, which consequently influenced its photocatalytic activity. Among the synthesized materials, GCN-550 exhibited the best performance, achieving approximately 90% degradation of methylene blue (MB) within 60 min, with an apparent rate constant of $0.0352 min^{-1}$. The superior activity was associated with its favourable structural and optical characteristics, including a relatively low band gap of 2.71 eV. Scavenging experiments revealed that superoxide radicals played the dominant role in MB degradation, while hydroxyl radicals and photogenerated holes also contributed to the process. Moreover, GCN-550 maintained approximately 78% degradation efficiency after four cycles, demonstrating satisfactory reusability. These findings highlight the importance of optimizing calcination temperature for tailoring the properties and photocatalytic performance of pristine g-C_3N_4 for wastewater treatment applications.

REFERENCES

Alwin, E., Kočí, K., Wojcieszak, R., Zieliński, M., Edelmannová, M., & Pietrowski, M. (2020). Influence of high temperature synthesis on the structure of graphitic carbon nitride and its hydrogen generation ability. *Materials*, 13(12), 2756. https://doi.org/10.3390/ma13122756

Anwer, H., Mahmood, A., Lee, J., Kim, K. H., Park, J. W., & Yip, A. C. (2019). Photocatalysts for degradation of dyes in industrial effluents: Opportunities and challenges. *Nano Research*, 12(5), 955-972. https://doi.org/10.1007/s12274-019-2287-0

Danbature, W. L., Isyaka, M. S., Abdullahi, M. A., Gambo, A. A., & Abdulmalik, S. S. (2023). Uv-Vis, Ftir and Xrd Characterization of Synthesized Magnetic Cobalt (Co3O4) Nanoparticle Used in Catalytic Decomposition of Hydrogen Peroxide. *FUDMA Journal of Sciences*, *7*(6), 222-227. https://doi.org/10.33003/fjs-2023-0706-2105

Donolikar, P. D., Sawant, V. A., Noda, K., & Sadale, S. B. (2025). Impact of synthesis temperatures on photocatalytic activity of graphitic carbon nitride. *Journal of Materials Science: Materials in Electronics*, 36(19), 1162. https://doi.org/10.1007/s10854-025-15231-x

Eswaran, P., Madasamy, P. D., Pillay, K., & Brink, H. (2025). Sunlight-driven photocatalytic degradation of methylene blue using ZnO/biochar nanocomposite derived from banana peels. *Biomass Conversion and Biorefinery*, 15(8), 12347-12367. https://doi.org/10.1007/s13399-024-05999-z

Gu, Q., Gao, Z., Zhao, H., Lou, Z., Liao, Y., & Xue, C. (2015). Temperature-controlled morphology evolution of graphitic carbon nitride nanostructures and their photocatalytic activities under visible light. *Rsc Advances*, 5(61), 49317-49325. https://doi.org/10.1039/c5ra07284k

Islam, R., Siddiqui, N. F. T., Tariq, M., Mahmood, K., Hussain, A., Hussain, S., & Sherazi, J. H. (2026). Fabrication of g-C_3N_4/Cu-MOF/Nd_2O_3@ NiO Nanocomposite for Dual Photocatalytic Applications: Methylene Blue Degradation and Hydrogen Peroxide Production. *Iranian Journal of Catalysis*, 16(1), 141-156. https://doi.org/10.57647/ijc.2026.1601.09

Ke, P., Zeng, D., Cui, J., Li, X., & Chen, Y. (2022). Improvement in structure and visible light catalytic performance of g-C_3N_4 fabricated at a higher temperature. *Catalysts*, 12(3), 247. https://doi.org/10.3390/catal12030247

Mallik, G., & Rath, S. (2022). Electrical properties of CuO nanoflakes/Au heterojunction under photo excitation. *Materials Today: Proceedings*, *62*, 5997–6000. https://doi.org/10.1016/j.matpr.2022.04.978

Michalska, M., Pavlovsky, J., Scholtzova, E., Skorna, P., Matejka, V., Bochenek, K., & Nishihara, H. (2024). A facile approach for fabricating g-C_3N_4-based materials as metal-free photocatalysts. *Results in Engineering*, 24, 103109. https://doi.org/10.1016/j.rineng.2024.103109

Mo, Z., She, X., Li, Y., Liu, L., Huang, L., Chen, Z., & Li, H. (2015). Synthesis of g-C_3N_4 at different temperatures for superior visible/UV photocatalytic performance and

photoelectrochemical sensing of MB solution. *RSC Advances*, *5*(123), 101552-101562. https://doi.org/10.1039/c5ra19586a

Nabeel, M. I., Ahmad, N., Arif, S., Hussain, D., & Musharraf, S. G. (2026). Facile two-step synthesis of yttrium-doped g-C_3N_4 for enhanced photocatalytic degradation of methylene blue with self-cleaning properties. *Nanoscale Advances*, 8(2), 565-579. https://doi.org/10.1039/d5na00600g

Nabi, G., Malik, N., & Raza, W. (2020). Degradation effect of temperature variation and dye loading g-C_3N_4 towards organic dyes. *Inorganic Chemistry Communications*, 119, 108050. https://doi.org/10.1016/j.inoche.2020.108050

Parmar, H., Majethia, K., Patel, J., Soni, D., Thaikoottathil, J. V., Taneja, N., & Gaur, R. (2026). Thiourea-derived g-C_3N_4 with time-tuned properties for efficient dye degradation and in vitro cytotoxicity evaluation. *Scientific Reports*, 16, 16711. https://doi.org/10.1038/s41598-026-47485-8

Paul, D. R., Sharma, R., Nehra, S. P., & Sharma, A. (2019). Effect of calcination temperature, pH and catalyst loading on photodegradation efficiency of urea derived graphitic carbon nitride towards methylene blue dye solution. *RSC advances*, 9(27), 15381-15391. https://doi.org/10.1039/c9ra02201e

Pourali, S., Amrollahi, R., Alamolhoda, S., & Masoudpanah, S. M. (2025). In situ synthesis of ZnO/g-C_3N_4 based composites for photodegradation of methylene blue under visible light. *Scientific Reports*, 15(1), 462. https://doi.org/10.1038/s41598-024-84645-0

Rafiq, A., Ikram, M., Ali, S., Niaz, F., Khan, M., Khan, Q., & Maqbool, M. (2021). Photocatalytic degradation of dyes using semiconductor photocatalysts to clean industrial water pollution. *Journal of Industrial and Engineering Chemistry*, 97, 111-128. https://doi.org/10.1016/j.jiec.2021.02.017

Rasheed, S., Khan, S. A., Nazir, M. A., Ali, S., Younas, M., Iqbal, R., & Rehman, A. U. (2024). Photocatalytic degradation of methylene blue by engineering tungstic acid@ ZIF-67 cocatalyst. *ChemistrySelect*, 9(46), e202403807. https://doi.org/10.1002/slct.202403807

Roškarič, M., Žerjav, G., Zavašnik, J., & Pintar, A. (2022). The influence of synthesis conditions on the visible-light triggered photocatalytic activity of g-C_3N_4/TiO_2 composites used in AOPs. *Journal of Environmental Chemical Engineering*, 10(3), 107656. https://doi.org/10.1016/j.jece.2022.107656

Sewnet, A., Alemayehu, E., Abebe, M., Mani, D., Thomas, S., Kalarikkal, N., & Lennartz, B. (2023). Single-step synthesis of graphitic carbon nitride nanomaterials by directly calcining the mixture of urea and thiourea: Application for Rhodamine B (RhB) dye degradation. *Nanomaterials*, 13(4), 762. https://doi.org/10.3390/nano13040762

Speltini, A., Pisanu, A., Profumo, A., Milanese, C., Sangaletti, L., Drera, G., & Malavasi, L. (2018). Rationalization of hydrogen production by bulk g-C_3N_4: an in-depth correlation between physico-chemical parameters and solar light photocatalysis. *RSC Advances*, *8*(69), 39421-39431. https://doi.org/10.1039/c8ra08880b

Tibebu, S., Gnaro, M. A., Kebede, A. M., Ammona, A. A., Sime, T., Ayalneh, S., & Jabli, M. (2025). Efficient photocatalytic degradation of methylene blue using Arundo donax biochar/graphitic carbon nitride composite. *Results in Engineering*, 28, 108143. https://doi.org/10.1016/j.rineng.2025.108143

Wang, S., Li, F., Dai, X., Wang, C., Lv, X., Waterhouse, G. I., & Ai, S. (2020). Highly flexible and stable carbon nitride/cellulose acetate porous films with enhanced photocatalytic activity for contaminants removal from wastewater. *Journal of Hazardous Materials*, 384, 121417. https://doi.org/10.1016/j.jhazmat.2019.121417

Wudil, Y. S., Ahmad, U. F., Gondal, M. A., Al-Osta, M. A., Almohammedi, A., Sa'id, R. S., & Mohamed, M. J. S. (2023). Tuning of graphitic carbon nitride (g-C_3N_4) for photocatalysis: a critical review. *Arabian Journal of Chemistry*, 16(3), 104542. https://doi.org/10.1016/j.arabjc.2023.104542

Zheng, W., Ye, C., Yu, M., Yang, S., Xiu, Y., He, X., & Wang, L. (2025). Fabrication of metal-doped graphite phase carbon nitride-based membrane and its application. *Advanced Composites and Hybrid Materials*, 8(1), 61. https://doi.org/10.1007/s42114-024-01175-z